Acta Crystallographica Section A
Foundations of Crystallography
ISSN 0108-7673

Received 27 September 2010
Accepted 13 December 2010

Importance of the consideration of anharmonic motion in charge-density studies: a comparison of variable-temperature studies on two explosives, RDX and HMX

Vladimir V. Zhurov,[a] Elizabeth A. Zhurova,[a] Adam I. Stash[b] and A. Alan Pinkerton[a]*

[a]Department of Chemistry, The University of Toledo, Toledo, OH 43606, USA, and [b]Karpov Institute of Physical Chemistry, Moscow, Russia. Correspondence e-mail: apinker@uoft02.utoledo.edu

Extremely accurate X-ray data were obtained for the explosive RDX (hexahydro-1,3,5-trinitro-1,3,5-triazine) at three different temperatures (20, 120 and 298 K). Collected reflections were integrated using the latest version of the program *VIIPP* which uses separate $K\alpha_1/K\alpha_2$ contributions to the profile fitting during integration. For each temperature both anharmonic and harmonic descriptions of the atomic thermal motion were utilized in the model refinements along with the multipole expansion of the electron density. H atoms were refined anisotropically and agree well with a previous neutron study. Topological analysis [Bader (1990). *Atoms in Molecules: A Quantum Theory. The International Series of Monographs of Chemistry*, edited by J. Halpern & M. L. H. Green. Oxford: Clarendon Press] of the attained electron density followed. For 1,3,5,7-tetranitro-1,3,5,7-tetraazacyclooctane (HMX), old data collected at 20 and 120 K were re-integrated with the new version of *VIIPP* and refined in the same manner as for RDX. In both cases theoretical structure factors were also calculated based on the 20 K structures, and employed in comparison multipole refinements for the atoms at rest. Limiting the refinement to a harmonic model of the atomic displacements may result in a biased and erroneous electron density, especially when atomic vibrations are significant (as in RDX) and at temperatures higher than obtained by using liquid helium. Given the similarity of the two compounds the effects of anharmonic motion are strikingly more severe in the case of RDX. Our study reinforces the conclusion of Meindl *et al.* [*Acta Cryst.* (2010), A**66**, 362–371] that in certain cases it is necessary to include anharmonic term(s) of the probability density function (or temperature factor) in order to obtain a meaningful electron density suitable for topological analysis, even for compact (high-density) light-atom structures. For RDX it was observed that the oxygen lone-pair concentrations of electrons are located close to perpendicular to the N—O bond vectors, which is typical for explosive materials. Conjugation of the electron density in the $-N-NO_2$ fragment has been established based on the topological bond orders. Nine moderately strong hydrogen bonds and nine N—N, O—N and O—O bonding interactions were found and described. The RDX molecular electronic energy per mole is 4.02–4.04 a.u., very close to the reported value for HMX.

1. Introduction

Hexahydro-1,3,5-trinitro-1,3,5-triazine (RDX) is one of the most widely used explosives in military applications today. The extensive use of RDX stems from its relative insensitivity to external conditions, high performance level and reasonably inexpensive synthesis (Davidson *et al.*, 2008; Ciezak *et al.*, 2007, and references therein). For an explosive it is only a moderately shock-sensitive material (h_{50} = 24 cm; Storm *et al.*, 1990),[1] which makes it a suitable object for an X-ray diffraction study.

Four different RDX polymorphs are known with only one (α form) being stable at ambient and low temperatures and at ambient pressure (Davidson *et al.*, 2008; Ciezak *et al.*, 2007;

[1] The shorter the impact drop height, h_{50}, the greater is the sensitivity.

Vladimiroff & Rice, 2002). The structure of orthorhombic α-RDX (space group *Pbca*) was previously determined both by neutron diffraction (Choi & Prince, 1972) and from X-rays (Harris & Reed, 1959; Hakey *et al.*, 2008).

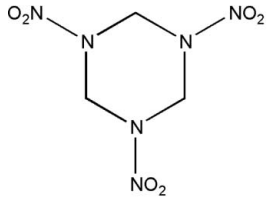

RDX

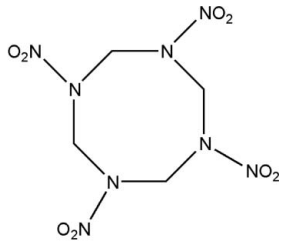

HMX

In this paper we present results from charge-density studies for the α phase of RDX at three different temperatures: 20 K measured with liquid helium, 120 K measured with liquid nitrogen, and at room temperature. The results are compared with analogous studies of the explosive HMX (1,3,5,7-tetranitro-1,3,5,7-tetraazacyclooctane) (with similar shock sensitivity[2]) measured at 20 and 120 K. The HMX helium-temperature charge-density study was reported earlier (Zhurova *et al.*, 2007). For a better description of physical effects in a crystal we have utilized a model accounting simultaneously for the asphericity of the electron density, anharmonic 'heavy-atom' nuclear displacements and anisotropic H-atom motion. The approach combining the simultaneous refinement of a multipole model and anharmonic atomic displacement parameters has not always been well accepted in the crystallographic community. For example, Mallinson *et al.* (1988) claimed that, although anharmonic displacements can be modeled by multipole model parameters, and although simultaneous refinement of anharmonic and aspherical effects is possible, the resulting separation may not be accurate. Restori & Schwarzenbach (1996) stated that, particularly for heavy atoms, anharmonic nuclear motion and aspherical electron-density features cannot be distinguished from each other by an X-ray experiment at a single temperature. However, for a very heavy atom (Th) on a special position, Iversen *et al.* (1999) reported the separation of anharmonic nuclear motion from electron-deformation effects using very high resolution X-ray data sets at very low (liquid-helium) temperatures. Ivanov *et al.* (1999), Zhurova *et al.* (2000), Tsirelson *et al.* (2003) and Zhurova & Tsirelson (2002) also successfully separated the anharmonic thermal motion and the asphericity of the electron density in $KNiF_3$, $KTaO_3$ and MgB_2 at room temperature, and in $SrTiO_3$ at 145 K.[3] A recent study on a 1,10-phenanthroline zinc thiolate complex (Scheins *et al.*, 2010) demonstrated the importance of accounting for anharmonic motion of the Zn atom in order to obtain a reliable description of the electron density. Meindl *et al.* (2010) recently demonstrated that 'the neglect of anharmonic nuclear motion leads to a characteristic imprint onto the residual density distribution in terms of residual density peaks and holes, in terms of the whole residual density distribution and in terms of the number, location and strength of valence-shell charge concentrations'. It might be argued that the previous successful deconvolution of the anharmonic motion from the aspherical valence density is due to the higher contribution of the core electron scattering in these medium- to heavy-atom structures. However, Birkedal *et al.* (2004) demonstrated that a combined anharmonic motion/multipole refinement is possible for light-atom structures (urea) given extremely accurate diffraction data.

In 1976, Hirshfeld declared that hydrogen displacement parameters cannot be derived from X-ray data because of large deformation densities at the nuclei (Hirshfeld, 1976). Since then, the overwhelming majority of charge-density studies employed an isotropic model of the H-atom thermal displacements with H atoms positioned at average neutron distances (Munshi *et al.*, 2008). Although this rough model works reasonably well, it may introduce a bias into the electron density and derived properties (Roversi & Destro, 2004; Madsen *et al.*, 2004). Certainly, hydrogen anisotropic displacement parameters (ADPs) can be obtained from a neutron diffraction experiment on the same compound (see, for example, Piccoli *et al.*, 2008), but, owing to a possible difference in the exact temperature of the experiments, crystal quality and other issues, scaling of hydrogen ADPs may be necessary (Blessing, 1995), which is another source of data bias. Obtaining accurate neutron data for the same compound may also be a problem, especially for an unstable or explosive compound. Three different approaches to artificially model anisotropic hydrogen motion were published recently in an attempt to circumvent this problem. Roversi & Destro (2004) approximated hydrogen ADPs as a sum of two terms coming from the external (TLS) and intramolecular motions, where estimates of internal contributions were deduced from mean-square amplitudes of motion for approximate vibrational modes and frequencies obtained from solid-state infrared spectra. Although this model can be widely applicable, it relies on the availability of solid-state spectroscopic data or, in their absence, the transferability of frequencies and normal modes from an isolated molecule to the molecule in the solid state (Munshi *et al.*, 2008). Madsen *et al.* (2004) proposed obtaining the internal mode contribution from an analysis of ADPs derived from neutron diffraction data. The approach was implemented through the web-accessible program *SHADE* (Madsen, 2006). This method also relies on the transferability of internal mean-square displacements from one crystal to another. Our personal experience with *SHADE* shows that, although the resulting hydrogen anisotropic thermal ellipsoids may look reasonable, their introduction into the model may increase the *R* value in the multipole refinement by 0.4–0.5%. Whitten & Spackman (2006) have suggested obtaining information on internal vibrational motion from *ab initio* cluster calculations using the ONIOM approach (Svensson *et al.*, 1996). This method requires a periodic Hartree–Fock calculation on the crystal, as well as an ONIOM geometry optimization of a cluster, typically of $\sim$15 molecules (Munshi *et*

[2] HMX: h_{50} = 26, 32 cm (Storm *et al.*, 1990; Simpson *et al.*, 1997).
[3] This list is by no means complete.

Table 1
Experimental details.

	RDX, 20.0 (1) K	RDX, 120.0 (2) K	RDX, 298 K	HMX, 20 (2) K	HMX, 120.0 (1) K
Empirical formula	$C_3H_6O_6N_6$	$C_3H_6O_6N_6$	$C_3H_6O_6N_6$	$C_4H_8O_8N_8$	$C_4H_8O_8N_8$
Crystal size (mm)	0.23 × 0.23 × 0.23	0.29 × 0.29 × 0.17	0.29 × 0.29 × 0.29	0.26 × 0.26 × 0.12	0.41 × 0.42 × 0.42
Crystal shape	Pyramid	Prism	Pyramid	Prism	Prism
Wavelength (Å)	0.71073	0.71073	0.71073	0.71073	0.71073
Crystal system	Orthorhombic	Orthorhombic	Orthorhombic	Monoclinic	Monoclinic
Space group	*Pbca*	*Pbca*	*Pbca*	$P2_1/n$	$P2_1/n$
Unit-cell dimensions (Å, °)	a = 11.3790 (2), b = 10.5694 (2), c = 13.1314 (2)	a = 11.4425 (3), b = 10.6106 (3), c = 13.1558 (4)	a = 11.6103 (4), b = 10.7291 (3), c = 13.2013 (4)	a = 6.5209 (2), b = 10.7610 (2), c = 7.3062 (2), β = 102.058 (2)	a = 6.5250 (2), b = 10.8249 (2), c = 7.3175 (1), β = 102.256 (2)
V (Å^3), Z	1579.30, 8	1597.27, 8	1644.46, 8	501.37, 2	505.07, 2
μ (mm^{-1})	0.18	0.18	0.18	0.19	0.19
D_{calc} (g cm^{-3})	1.869	1.847	1.794	1.962	1.948
$(\sin\theta/\lambda)_{max}$ (Å^{-1})	1.322	1.293	0.931	1.329	1.330
Reflections integrated	120142	173199	238374	47712	70734
R_{int}/average data multiplicity	0.0191/11.3	0.0163/14.1	0.0167/44.1	0.0179/6.9	0.0168/10.6
Completeness					
$\sin\theta/\lambda < 0.67$ Å^{-1} (%)	100	100	100	98.6	97.7
all data (%)	69.8	85.1	96.8	70.4	67.4
Independent reflections	10651	12304	5403	6942	6702
Reflections used ($I > 3\sigma$)	8057	7986	3943	5650	5691
Refinement based on	F^2	F^2	F	F^2	F^2
Total number of parameters†	754/604	754/604	859/604	505/405	505/405
Weighting scheme: a, b†‡	0.006, 0.008/ 0.006, 0.012	0.008, 0.012/ 0.012, 0.015	0.005, 0.006/ 0.015, 0.056	0.008, 0.008/ 0.008, 0.008	0.004, 0.005/ 0.006, 0.006
Final $R(F^2)$†	0.0138/0.0143	0.0125/0.0149	0.0070/0.0159	0.0166/0.0169	0.0130/0.0145
$R_w(F^2)$†	0.0205/0.0221	0.0258/0.0322	0.0147/0.0391	0.0268/0.0275	0.0182/0.0231
$R(F)$†	0.0145/0.0149	0.0166/0.0182	0.0100/0.0178	0.0150/0.0154	0.0108/0.0121
$(\Delta/\sigma)_{max}$†	1.9×10^{-7}/ 1.4×10^{-6}	1.2×10^{-6}/ 3.4×10^{-9}	2.5×10^{-9}/ 5.3×10^{-9}	2.0×10^{-12}/ 3.7×10^{-12}	1.3×10^{-12}/ 3.3×10^{-12}
$\Delta\rho$†$_{min-max}$ (e Å^{-3})	−0.170–0.186/ −0.203–0.192	−0.150–0.137/ −0.182–0.177	−0.054–0.056/ −0.105–0.153	−0.123–0.119/ −0.203–0.212	−0.102–0.114/ −0.140–0.127

† Anharmonic/harmonic refinements. ‡ $w = 1/[\sigma^2(F^2) + (aF_{obs}^2)^2 + bF_{obs}^2]$.

al., 2008). Finally, a rigid-body model used to estimate external motion in all three approaches is not always exactly applicable.

Recently we have demonstrated for several crystals (Zhurov *et al.*, 2011) that, given a very accurate data set, it is possible (and necessary) to refine H atoms anisotropically, at least for relatively small molecules. Thus, in the current work, we have refined multipole model parameters along with anharmonic displacement parameters for 'heavy' atoms, and anisotropic displacement parameters for H atoms. A comparison of the results at different temperatures, with theoretical data, with a neutron diffraction experiment, and with another similar explosive compound (HMX) is presented below.

2. Experimental

2.1. Data collection and reduction

Different samples were used for all five experiments. In each case a regularly shaped crystal (Table 1), crystallized from warm (RDX) or hot (HMX) acetone, was mounted on the top of a glass capillary. An Oxford Cryostream device was utilized to cool a crystal down to 120 K, and an open-flow helium cryostat (Hardie *et al.*, 1998; Kirschbaum *et al.*, 1999; Ribaud *et al.*, 2001) was used to reach a sample temperature of 20 K. X-ray diffraction measurements were performed with a Rigaku R-Axis Rapid diffractometer with a high-power Mo rotating-anode generator (18 kW), graphite monochromator and a curved image-plate detector. In order to avoid significant overlap of reflections in any one image, a 4° ω-scan range was chosen. To facilitate interframe scaling, oscillation ranges for adjacent images were overlapped by 2°, thus each 180° run consisted of a total of 89 images.

2.1.1. RDX at 20 K. Four complete runs covering 0−180° in ω were collected at different χ and φ settings, two at $\chi = 0°$ ($\varphi = 0, 180°$) and two at $\chi = 30°$ ($\varphi = 0, 180°$). In order to avoid saturation of the strongest reflections, a 100 s exposure time per image was chosen.

2.1.2. RDX at 120 K. A total of eight runs were collected with two at $\chi = 0°$ ($\varphi = 0, 180°$) and two at $\chi = 20°$ ($\varphi = 0, 180°$) measured for 55 s, and the same sets were measured again for 240 s to improve the statistics for weak reflections. No significant 'bleeding' was observed for the longer exposures.

2.1.3. RDX at room temperature. A total of ten runs were collected with two at $\chi = 0°$ ($\varphi = 0, 180°$), four at $\chi = 20°$ ($\varphi = 0$, 90, 180, 270°) and four at $\chi = 40°$ ($\varphi = 0$, 90, 180, 270°), measured for 720 s.

2.1.4. HMX at 20 K. A total of four runs were collected with two at $\chi = 0°$ ($\varphi = 0, 180°$) and two at $\chi = 20°$ ($\varphi = 0, 180°$), measured for 70 s (Zhurova *et al.*, 2007).

2.1.5. HMX at 120 K. A total of nine runs were collected with two at $\chi = 0°$ ($\varphi = 0, 180°$), two at $\chi = 20°$ ($\varphi = 0, 180°$) and

one at $\chi = 10^\circ$ ($\varphi = 0^\circ$) measured for 150 s, two at $\chi = 0^\circ$ ($\varphi = 0$, 180°) and one at $\chi = 10^\circ$ ($\varphi = 0^\circ$) measured for 20 s, and one at $\chi = 20^\circ$ ($\varphi = 0^\circ$) measured for 40 s. No significant 'bleeding' was observed for longer exposures.

The experimental strategy was chosen differently for different crystals for methodological and instrument testing reasons, but, at the end, all measured data were used for the charge-density refinements.

The collected data were integrated using a new version of the program *VIIPP* (Zhurov *et al.*, 2005; Zhurova *et al.*, 1999) using the predicted reflection positions from the program *HKL2000* (Otwinowski & Minor, 1997). The integrated data quality was greatly improved over earlier versions of *VIIPP* by using separate extracted $K\alpha_1/K\alpha_2$ parts both for creating a standard profile and for profile adjustment within the integration box during the fitting and integration procedure. Partial and overlapped reflections were rejected during the integration process. Data have been corrected for Lorentz–polarization effects, whereas effects of absorption and thermal diffuse scattering were ignored. Data were scaled and then averaged using the program *SORTAV* (Blessing, 1987). Most of the scaling factors for different images with the same exposure time were very close to unity (usually within 1%; however, in several cases differences of up to 4.1% were observed). Extreme outliers (about 0.5%) were rejected during averaging. Not surprisingly, there was no observable data at room temperature beyond $\sin\theta/\lambda = 0.931$ Å^{-1}, and integration was only carried out up to this limit. Other experimental details are listed in Table 1.

3. Refinements

The RDX crystal structure has been reported previously (Harris & Reed, 1959; Choi & Prince, 1972; Hakey *et al.*, 2008). From our experimental data the crystal structure was resolved by direct methods and a preliminary least-squares refinement was carried out using the *SHELXTL* program suite (Sheldrick, 2008). A multipole model refinement (Hansen & Coppens, 1978) using the *XD* program package (Volkov *et al.*, 2006) was performed for both experimental and solid-state theoretical (see below) data. Two models were refined for each experiment with anharmonic and harmonic descriptions of the atomic displacements for the non-H atoms, and anisotropic vibrations for the latter. Anharmonicity of the third order was considered to adequately describe the atomic thermal motion at 20 and 120 K, whereas third and fourth orders were necessary for the description at room temperature where atomic displacements are much higher. The multipole model for all non-H atoms was refined up to the hexadecapole level, while for the H atoms only three dipoles and the Q0 quadrupole were refined. Chemical constraints for similar atoms were applied at the initial stages of refinements. Then, these constraints were gradually released, and the final model was refined unconstrained in each case. The molecular electroneutrality requirement was applied in all cases. A total of five each of the expansion–contraction parameters, κ and κ', were utilized (five atom types) in order to allow the necessary flexibility while attempting to maintain a minimum number of parameters. First, the C—H bond lengths were fixed to the tabulated (Allen & Bruno, 2010) neutron values, and the first kappa parameter (κ) for H atoms was refined. Hydrogen κ' was set to 1.2. After convergence, the H-atom κ was fixed, and C—H distances were allowed to vary. Highly correlated parameters (such as anharmonic displacement and multipole parameters) were refined in separate groups. In the final stage a full matrix refinement was performed, including all H-atom coordinates (without constraints) and κ(H). The refinement procedure was stable, and full convergence of all parameters was reached (Table 1). In the case of the anharmonic refinement using room-temperature data, mirror symmetry was imposed on the multipole parameters of the O and N atoms. The mirror planes are defined as perpendicular to the NO_2 plane through the corresponding N—O or N—N bonds. In the final harmonic room-temperature refinement all multipole parameters were allowed to refine, but both κ and κ' for H atoms were set to 1.2, and C—H bond lengths were still constrained as before.

The rigid-bond test (Hirshfeld, 1976) showed that the differences of mean-square displacement amplitudes along the interatomic vectors for non-H atoms were less than 6×10^{-4} Å^2 at low temperatures and less than 5.0×10^{-3} Å^2 for RDX at 298 K. Averaged ratios (in 0.05 Å^{-1} bins) of observed and calculated structure factors were very close to unity (all data within 3% and up to $\sin\theta/\lambda = 1.2$ Å^{-1} within 1.0%) indicating a correct scale factor for all data, as well as good model fitting for the whole $\sin\theta/\lambda$ range. The minimum and maximum values of the residual electron density ($\delta\rho_{\rm resid} = \rho_{\rm exper} - \rho_{\rm mult}$) are listed in Table 1 (calculated with all data). The total electron density was non-negative everywhere for all refinements, except for the harmonic model at room temperature, where relatively small negative areas were found. Therefore, the $\rho(r)$ distribution and the multipole model obtained in the harmonic refinement for 298 K can be considered to be meaningless, but were included in further calculations for comparison purposes. The previously recorded (Zhurova *et al.*, 2007) data for HMX at 20 K and 120 K have been re-integrated using the latest version of the program *VIIPP*, and re-refined in the same manner as the RDX experiments.

3.1. Theoretical calculations

A DFT B3LYP periodic theoretical calculation for RDX was performed using the program *CRYSTAL98* (Saunders *et al.*, 1998). The 6-311G(d,p) basis set was used with the molecular geometry fixed at that observed experimentally at 20 K. Theoretical structure factors were calculated for all possible *hkl* indices (14 531 reflections) up to $\sin\theta/\lambda = 1.3$ Å^{-1}, and used for multipole refinements in a similar manner as for the experimental data, but with all ADPs set to zero. A final $R(F) = 0.0055$ was reached. The results from similar HMX theoretical calculations were reported previously (Zhurova *et al.*, 2007).

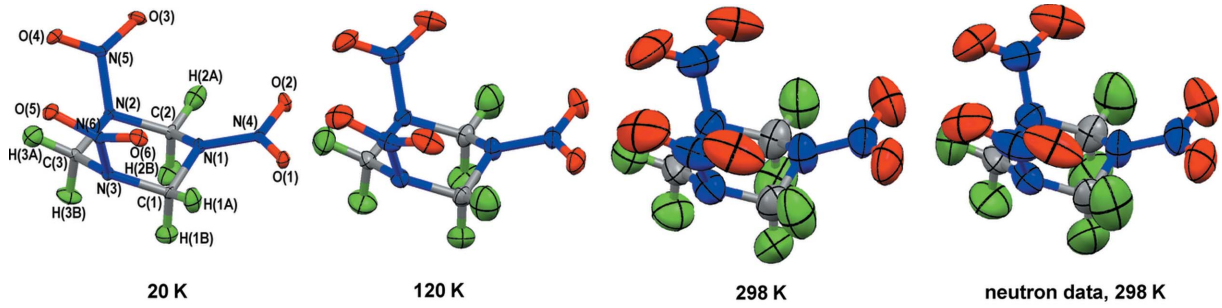

Figure 1
RDX atomic thermal ellipsoids at the 75% probability level derived from our anharmonic model refinements and from the harmonic refinement using neutron data (Choi & Prince, 1972).

The electron density in the RDX and HMX crystals at various temperatures was reconstructed and analyzed using the program packages *XDPROP*, *TOPXD* (Volkov *et al.*, 2006) and *WinXPRO* (Stash & Tsirelson, 2002, 2005).

4. Results and discussion

The chair conformation of the α-RDX molecule with two of the nitro groups in pseudo-axial positions and the other in a pseudo-equatorial position is shown in Fig. 1. Fig. 2 shows the packing diagram projected down the *b* axis with hydrogen bonds shown as dashed green lines.

Some preliminary electron-density results for RDX obtained in our laboratory at 90 K have been previously reported (Chen, 2004). From our new data, 75% thermal probability ellipsoids as extracted from anharmonic refinements at all three temperatures are shown in Fig. 1 along with those obtained from a harmonic refinement using room-temperature neutron data (Choi & Prince, 1972). All ellipsoids, including those for H atoms, look reasonable for all temperatures. In particular, as shown in Fig. 1, there is very good agreement between the X-ray and neutron (Choi & Prince, 1972) room-temperature atomic ellipsoids (U_{ij}'s have been deposited). Indeed, the average difference in U_{ij}'s for H atoms derived from the harmonic X-ray and neutron refinements is 2.3 s.u. (the s.u.'s being taken from the neutron refinement). For comparison, the average difference in U_{ij}'s for O atoms is 1.5 s.u., for N atoms 1.2 s.u., and for C atoms 1.1 s.u. Thermal ellipsoid plots from the RDX harmonic refinements and HMX refinements have also been deposited.[4]

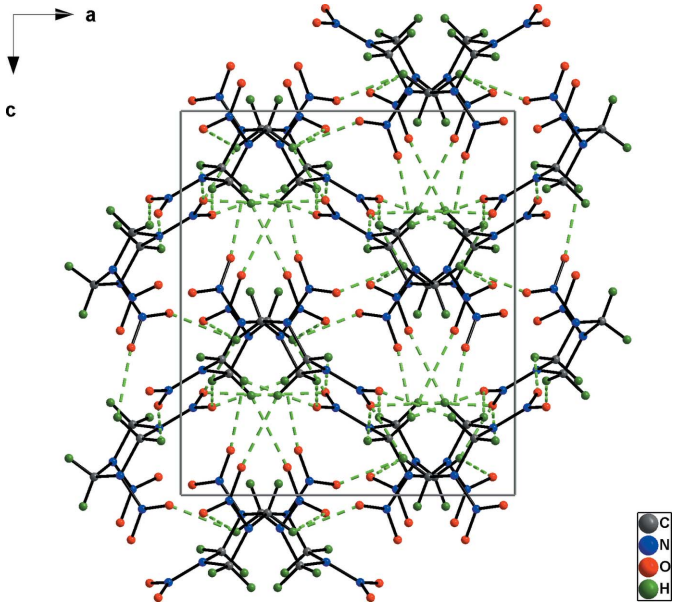

Figure 2
α-RDX packing diagram with hydrogen bonds shown as dashed green lines. Projection down the *b* axis.

Table 2
RDX C—H bond distances (Å) obtained from various refinements.

1: 20 K, anharmonic refinement; 2: 20 K, harmonic refinement; 3: 120 K, anharmonic refinement; 4: 120 K, harmonic refinement; 5: 298 K, anharmonic refinement.

Bond	1	2	3	4	5
C(1)—H(1*A*)	1.070 (12)	1.069 (12)	1.066 (16)	1.083 (16)	1.063 (14)
C(1)—H(1*B*)	1.085 (10)	1.089 (11)	1.072 (13)	1.064 (16)	1.090 (12)
C(2)—H(2*A*)	1.059 (13)	1.056 (13)	1.044 (15)	1.052 (16)	1.063 (13)
C(2)—H(2*B*)	1.089 (11)	1.088 (11)	1.088 (13)	1.089 (15)	1.105 (12)
C(3)—H(3*A*)	1.058 (11)	1.056 (12)	1.080 (13)	1.079 (14)	1.087 (10)
C(3)—H(3*B*)	1.079 (10)	1.077 (11)	1.091 (12)	1.096 (14)	1.085 (10)

Estimated C—H bond lengths in RDX are listed in Table 2; those in HMX have been deposited. In the case of the harmonic refinement using room-temperature data the refined C—H bond distances appeared to be unreasonable, thus the average neutron length was kept in the final refinement model at this temperature. At low temperatures the C—H bond lengths were ~0.017 Å shorter (on average) than the reported (Allen & Bruno, 2010) average Z_2–Csp^3–H_2 neutron distance. Our result is in very good agreement with the RDX neutron diffraction study (Choi & Prince, 1972), where the C—H bond lengths were reported in the range 1.058–1.092 Å. Thus, both hydrogen atomic positions and their anisotropic thermal motion were extracted cleanly from the X-ray data.

Most of the refined 'heavy-atom' anharmonic parameters appeared to be above their standard uncertainties with the

[4] Supplementary data for this paper are available from the IUCr electronic archives (Reference: SH5121). Services for accessing these data are described at the back of the journal.

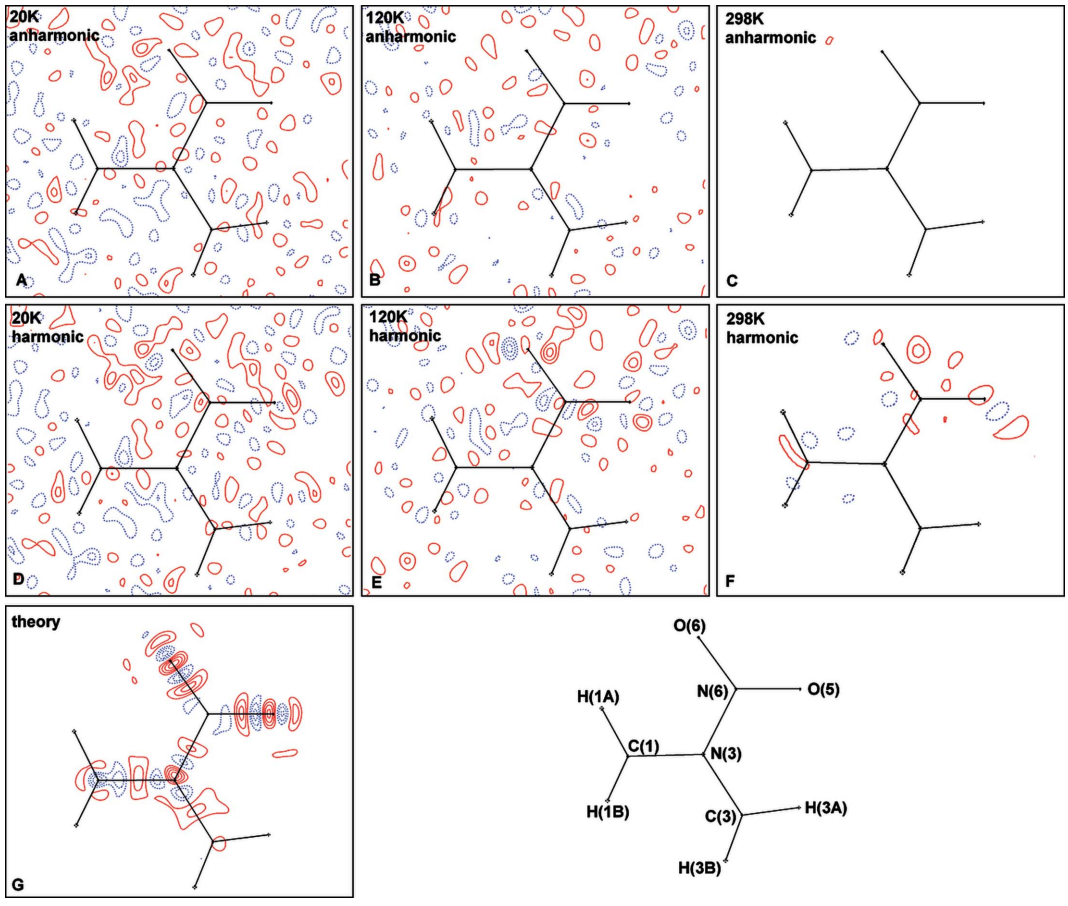

Figure 3
Residual electron density maps of RDX in the plane of the N(6)—O(5)—O(6) group. A: anharmonic model refinement at 20 K; B: anharmonic refinement at 120 K; C: anharmonic refinement at 298 K; D: harmonic model refinement at 20 K; E: harmonic refinement at 120 K; F: harmonic refinement at 298 K; G: multipole model refinement on theoretical data. Contour intervals are 0.05 e Å^{-3}. Positive contours are red and negative contours are blue dashed lines. In the case of the room-temperature anharmonic refinement (C) the residual density was less than ±0.05 e Å^{-3} in this particular plane. See Table 1 for minimum/maximum densities in all cases.

highest values for the O atoms, as expected. Limiting the number of anharmonic parameters by setting statistically insignificant parameters to zero did not provide any improvement of the model, so all of the parameters were allowed to refine. Their values can be found in the deposited CIF file. Total single-particle vibrational probability density function maps for O atoms at room temperature have also been deposited.

RDX residual electron-density maps calculated with all data are shown in Fig. 3 in the plane of one of the nitro groups and additional maps have been deposited. In general, no significant features are observed in the bond or lone-pair areas. Less residual density is observed when the anharmonic model is refined, as expected, especially at the higher temperatures. The apparent clean residual map for the room-temperature study compared with the lower temperatures is due to the lack of measurable weak high-angle data ($\sin\theta/\lambda >$ 0.931 Å^{-1}), the presence of which engenders significant noise in the low-temperature experiments.[5] In the case of the theoretical data, a large number of very weak reflections contributed to the residual density observed. The deficiency of the multipole model is also manifest in this map.

Static (model) deformation electron density maps ($\delta\rho$ = $\rho_{\rm multipole} - \rho_{\rm spherical}$) for RDX and HMX and the corresponding Laplacian ($\nabla^2\rho$) maps for RDX in the planes of representative NO_2 groups are shown in Figs. 4–6. For the refinements based on the 20 K data, or the theoretical data, and for all refinements including anharmonic motion, each expected covalent bond manifests itself as a significant deformation electron density and a negative Laplacian peak. For the O atoms, electron concentrations associated with lone pairs are well defined and located close to perpendicular to the N—O bond vectors. A very similar picture has been observed previously for nitro groups in a number of other explosive (Zhurova & Pinkerton, 2001; Zhurova *et al.*, 2002, 2006, 2007; Ritchie *et al.*, 2003; Chen *et al.*, 2007) and non-explosive materials (Kubicki *et al.*, 2002; Volkov *et al.*, 2000; Messerschmidt *et al.*, 2002).

However, from the RDX refinements based on 120 K or room-temperature data, if thermal motion is described in the

[5] It is common practice in the charge-density field to limit the data used for calculating residual density maps to $\sin\theta/\lambda < 1.0$ Å^{-1}. Under these conditions all of the experimental residual maps reported here would be essentially featureless.

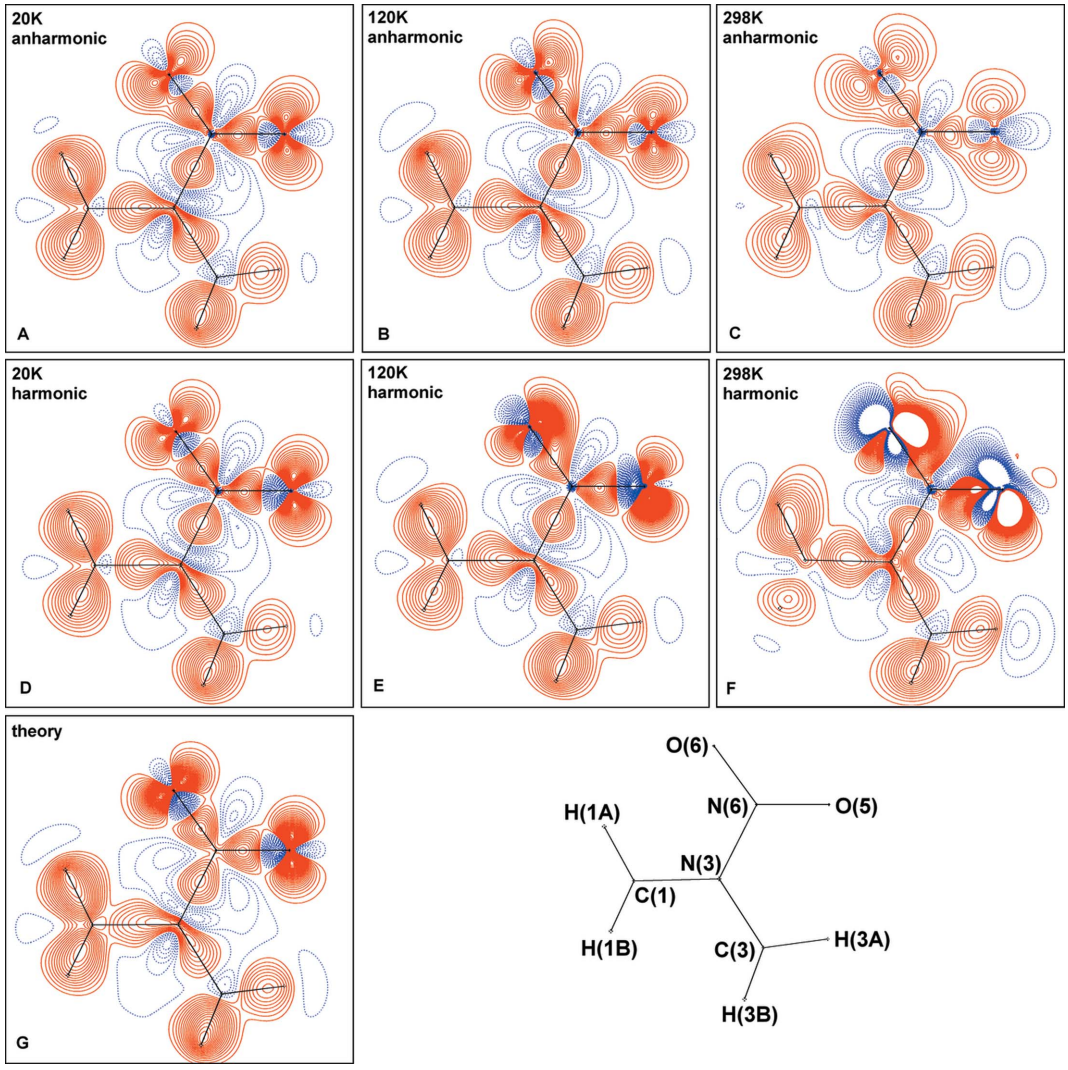

Figure 4
Deformation electron density maps of RDX in the plane of the N(6)—O(5)—O(6) group calculated in direct space using the program *XDPROP*. A: anharmonic model refinement at 20 K; B: anharmonic refinement at 120 K; C: anharmonic refinement at 298 K; D: harmonic model refinement at 20 K; E: harmonic refinement at 120 K; F: harmonic refinement at 298 K; G: multipole model refinement on theoretical data. Contour intervals are 0.05 e Å^{-3}. Positive contours are red and negative contours are blue dashed lines.

harmonic approximation an inaccurate and even erroneous electron density[6] is obtained. This can clearly be seen from the deformation electron density maps (Fig. 4), where unreasonably distorted peaks can be seen, especially in the region of oxygen lone pairs [Figs. 4(E) and 4(F)]. Anharmonic refinements at 120 K and at room temperature provided well defined peaks for all bonds and lone-pair concentrations of the electron density with somewhat lower peak heights compared with the theoretical calculation[7] [Figs. 4(B) and 4(C)]. Despite the higher atomic motion ($0.031 < U_{eq} < 0.068$), even room-temperature maps look reasonable when the anharmonic model is utilized. Thus, the possibility of studying the charge density of phases that are unstable at very low temperatures becomes viable when anharmonicity is taken into account.[8]

The Laplacian distribution (Fig. 5) follows the same trends as the deformation density, with distorted and shifted peaks around the O atoms after the harmonic refinements at 120 and 298 K, which then become much more reasonable when the anharmonicity is taken into account.

In the case of HMX, a very similar molecule to RDX, the picture is very different (Fig. 6). Reasonable deformation electron density maps were obtained from both harmonic and anharmonic refinements of data at 20 and 120 K.[9] As for RDX, most of the anharmonic parameters were statistically significant when refined; however, the effect on the maps is

[6] Note that negative areas in the total electron density were obtained in the case of harmonic refinements of the room-temperature data.
[7] All the maps were calculated in direct space using the multipole model parameters.
[8] This should not be taken as a recommendation for room-temperature charge density studies, as the lowest possible temperature will always provide a superior result.
[9] No room-temperature data are available.

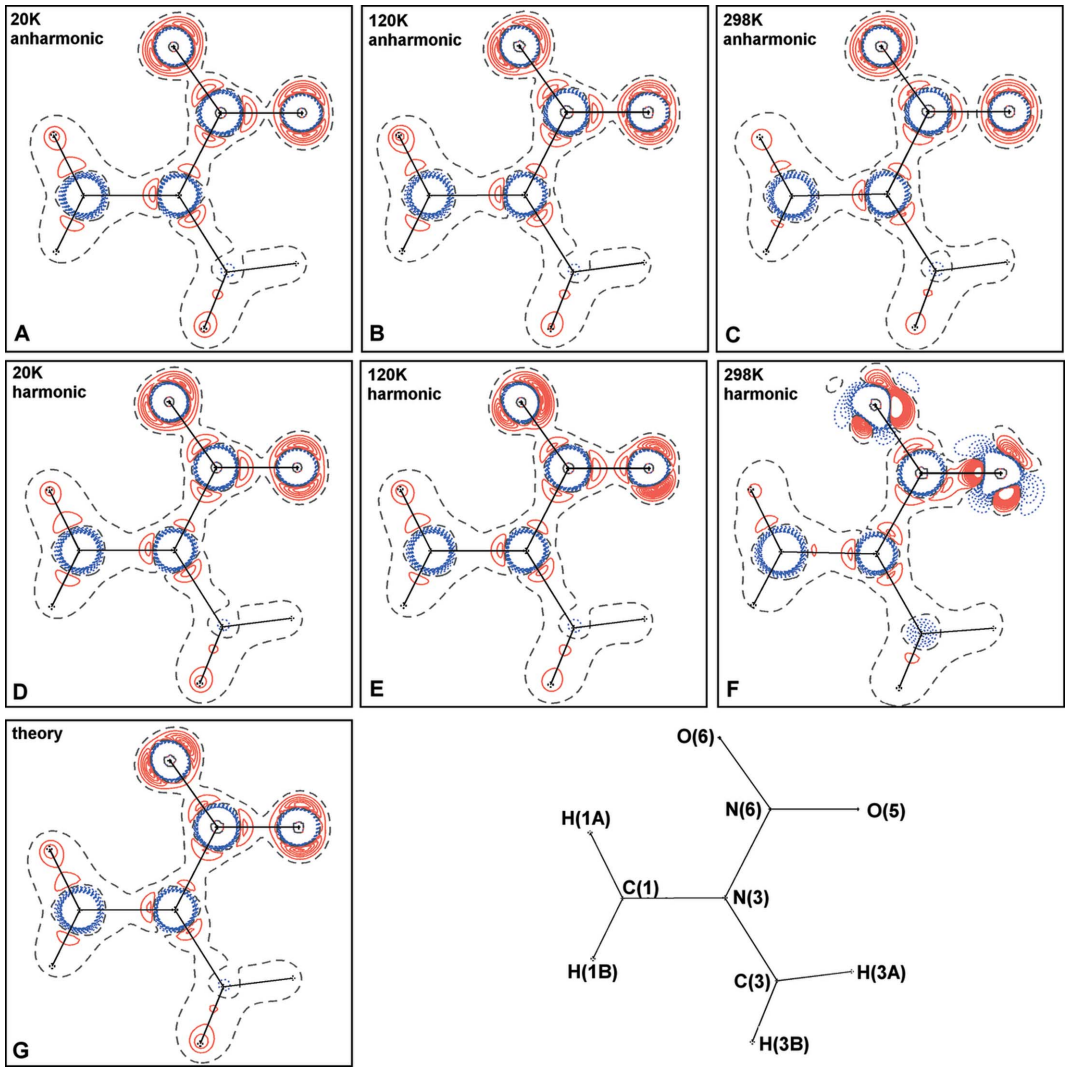

Figure 5
The Laplacian of the total electron density of RDX in the plane of the N(6)—O(5)—O(6) group: A: anharmonic model refinement at 20 K; B: anharmonic refinement at 120 K; C: anharmonic refinement at 298 K; D: harmonic model refinement at 20 K; E: harmonic refinement at 120 K; F: harmonic refinement at 298 K; G: multipole model refinement on theoretical data. Contour intervals are 25 e Å^{-5}. Negative contours are red and positive contours are blue dashed lines.

quite small. Although RDX and HMX have practically the same shock sensitivity, the HMX structure is more dense (Table 1) with shorter hydrogen bonds (Zhurova *et al.*, 2007). The more compact HMX crystal structure allows less atomic thermal motion, especially for the O atoms. Indeed, HMX atomic probability ellipsoids are much smaller than those in RDX at the same temperature (see deposited material). We thus conclude that in cases where atomic thermal motion is relatively high (even at 'cold' temperatures), such as in the RDX case, an anharmonic description of atomic thermal motion is necessary to obtain a meaningful electron-density distribution. When this atomic motion is somewhat restricted by the crystal packing, the harmonic description may be adequate (as in HMX). At the same time, *R* values and the residual electron density (Table 1) demonstrate the preference of an anharmonic refinement, even in the HMX case. Thus, a thorough analysis of different refinement strategies should be conducted before making a final decision.

Having demonstrated the importance of choosing an appropriate model for the thermal motion, it is instructive to examine the effects on the topology of the electron density and of the derived properties. Table 3 lists selected intramolecular (3,−1) bond critical points in RDX (the complete table has been deposited). Topological analysis of the electron density in HMX has been reported previously (Zhurova *et al.*, 2007) and will not be included in further analysis here. Not unexpectedly, the effects on bond lengths are minor, but it is satisfying to see that the most librational shortening of the O—N bonds at room temperature (0.030 Å compared with the 20 K refinements) is essentially removed by inclusion of the anharmonic terms (0.008 Å). As can be seen from Table 3, there is a quantitative difference in the electron density and the Laplacian values at the critical points between anharmonic and harmonic refinements at different temperatures, but there is no systematic trend. Typically inclusion of anharmonic displacements reduces the difference from the 20 K data to a

Table 3
Bond critical points in the RDX crystal: selected intramolecular bonds.

1: 20 K, anharmonic refinement; 2: 20 K, harmonic refinement; 3: 120 K, anharmonic refinement; 4: 120 K, harmonic refinement; 5: 298 K, anharmonic refinement; 6: 298 K, harmonic refinement; 7: theory; ρ is the electron density; $\nabla^2\rho$ is the Laplacian; R_{ij} is interatomic distance, d_1 and d_2 are the distances from the critical point to atoms 1 and 2, λ_1, λ_2, λ_3 are principal curvatures, ε is bond ellipticity, $n_{\rm topo}$ is topological bond order.

Bond		ρ (e Å^{-3})	$\nabla^2\rho$ (e Å^{-5})	R (Å)	d_1 (Å)	d_2 (Å)	λ_1 (e Å^{-5})	λ_2 (e Å^{-5})	λ_3 (e Å^{-5})	ε	$n_{\rm topo}$
O(5)—N(6)	1	3.333 (13)	−10.61 (5)	1.222	0.624	0.598	−30.186	−28.116	47.695	0.074	1.89
	2	3.349 (18)	−12.23 (8)	1.218	0.611	0.607	−30.067	−28.121	45.954	0.069	1.87
	3	3.431 (23)	−14.10 (8)	1.221	0.634	0.588	−30.939	−29.471	46.315	0.050	1.90
	4	3.551 (53)	−23.24 (21)	1.212	0.619	0.594	−33.307	−30.470	40.531	0.093	1.81
	5	3.198 (13)	−2.62 (4)	1.214	0.634	0.580	−25.847	−25.586	48.816	0.025	1.94
	6	4.037 (86)	−49.38 (25)	1.188	0.733	0.464	−47.398	−36.487	34.508	0.299	1.69
	7	3.270 (9)	−11.78 (4)	1.222	0.626	0.597	−28.890	−27.256	44.366	0.060	1.81
N(3)—N(6)	1	2.231 (17)	−8.46 (6)	1.403	0.685	0.718	−19.976	−16.229	27.750	0.231	1.22
	2	2.233 (15)	−8.59 (6)	1.404	0.680	0.724	−19.910	−16.095	27.415	0.237	1.24
	3	2.259 (20)	−9.80 (7)	1.403	0.682	0.722	−20.463	−16.303	26.964	0.255	1.22
	4	2.237 (18)	−8.89 (7)	1.404	0.684	0.721	−20.138	−15.946	27.193	0.263	1.24
	5	2.213 (24)	−6.91 (8)	1.394	0.689	0.706	−19.390	−15.542	28.022	0.248	1.30
	6	2.253 (36)	−8.71 (11)	1.401	0.703	0.699	−20.024	−15.916	27.232	0.258	1.28
	7	2.158 (8)	−5.77 (3)	1.403	0.681	0.722	−18.584	−15.067	27.878	0.233	1.30
N(3)—C(1)	1	1.802 (12)	−14.50 (4)	1.457	0.836	0.621	−13.483	−13.179	12.158	0.023	0.76
	2	1.799 (12)	−14.55 (4)	1.456	0.833	0.624	−13.445	−13.163	12.061	0.021	0.75
	3	1.820 (15)	−13.64 (5)	1.456	0.836	0.621	−13.401	−13.061	12.827	0.026	0.79
	4	1.824 (13)	−13.56 (5)	1.457	0.831	0.626	−13.395	−12.974	12.802	0.032	0.80
	5	1.739 (14)	−11.78 (4)	1.450	0.846	0.605	−11.722	−11.473	11.419	0.022	0.77
	6	1.932 (20)	−16.08 (8)	1.450	0.815	0.636	−14.677	−13.670	12.262	0.074	0.87
	7	1.737 (7)	−9.67 (2)	1.457	0.814	0.643	−12.896	−12.588	15.814	0.024	0.74
C(1)—H(1*A*)	1	1.921 (56)	−23.50 (23)	1.070	0.747	0.323	−19.901	−19.269	15.675	0.033	0.86
	2	1.900 (56)	−23.06 (26)	1.069	0.763	0.308	−20.017	−19.460	16.413	0.029	0.84
	3	1.971 (70)	−23.01 (24)	1.065	0.684	0.381	−18.906	−17.986	13.878	0.051	0.98
	4	1.887 (65)	−22.10 (25)	1.083	0.747	0.336	−18.983	−18.129	15.022	0.047	0.89
	5	1.832 (56)	−19.84 (21)	1.063	0.724	0.341	−17.493	−16.260	13.716	0.064	0.94
	6	1.795 (46)	−19.11 (19)	1.090	0.757	0.337	−18.233	−15.805	14.931	0.154	0.91
	7	2.023 (12)	−24.50 (5)	1.071	0.715	0.356	−20.600	−19.816	15.916	0.040	0.94

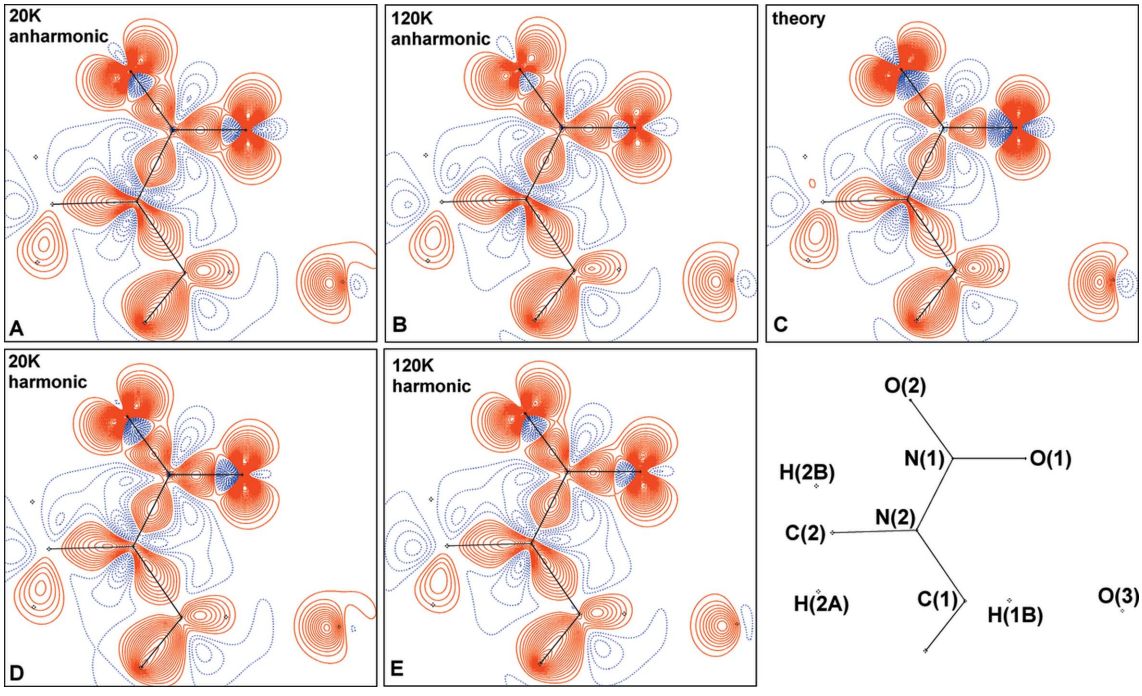

Figure 6
Deformation electron density maps of HMX in the plane of the N(1)—O(1)—O(2) group calculated in direct space using the program *XDPROP*. A: anharmonic model refinement at 20 K; B: anharmonic refinement at 120 K; C: multipole model refinement on theoretical data; D: harmonic model refinement at 20 K; E: harmonic refinement at 120 K. Contour intervals are 0.05 e Å^{-3}. Positive contours are red and negative contours are blue dashed lines.

Table 4
Bond critical points in the RDX crystal: hydrogen bonds.

All bond paths and virial paths have been verified. 1: 20 K, anharmonic refinement; 2: 20 K, harmonic refinement; 3: 120 K, anharmonic refinement; 4: 120 K, harmonic refinement; 5: 298 K, anharmonic refinement; 6: 298 K, harmonic refinement; 7: theory; ρ is the electron density; $\nabla^2\rho$ is the Laplacian; R_{ij} is the O···H interatomic distance, D_e is an approximate dissociation energy (Espinosa & Molins, 2000) calculated as $D_e = -v/2$, where v is the potential energy density.

	Bond	ρ (e Å^{-3})	$\nabla^2\rho$ (e Å^{-5})	R_{ij} (Å)	D_e (kJ mol^{-1})
1	O(1)···H(3*B*)—C(3)^{i}	0.075 (8)	0.959 (3)	2.401	8.53
2		0.076 (8)	0.957 (3)	2.404	8.66
3		0.063 (9)	0.901 (4)	2.402	7.22
4		0.060 (11)	0.895 (4)	2.398	6.96
5		0.062 (8)	0.816 (2)	2.472	6.74
6		0.065 (11)	0.721 (3)	2.471	6.63
7		0.069 (2)	0.906 (1)	2.401	7.78
1	O(2)···H(1*A*)—C(1)^{iv}	0.068 (8)	0.876 (2)	2.364	7.48
2		0.069 (8)	0.893 (2)	2.367	7.75
3		0.050 (11)	0.847 (4)	2.398	6.04
4		0.058 (10)	0.864 (3)	2.392	6.70
5		0.036 (8)	0.666 (3)	2.472	4.04
6		0.048 (9)	0.672 (4)	2.461	5.01
7		0.068 (2)	0.835 (1)	2.363	7.37
1	O(4)···H(2*B*)—C(2)^{ii}	0.061 (6)	0.920 (1)	2.452	7.22
2		0.062 (6)	0.926 (1)	2.453	7.22
3		0.057 (7)	0.888 (2)	2.470	6.70
4		0.056 (8)	0.905 (2)	2.474	6.70
5		0.053 (6)	0.767 (2)	2.499	5.85
6		0.040 (9)	0.733 (2)	2.497	4.76
7		0.062 (2)	0.990 (1)	2.451	7.42
1	O(1)···H(1*B*)—C(1)^{i}	0.059 (6)	0.812 (3)	2.501	6.56
2		0.058 (6)	0.801 (3)	2.500	6.43
3		0.063 (6)	0.777 (3)	2.544	6.70
4		0.061 (7)	0.749 (3)	2.549	6.30
5		0.053 (5)	0.773 (2)	2.600	5.43
6		0.042 (10)	0.574 (2)	2.586	4.21
7		0.053 (2)	0.770 (1)	2.501	5.86
1	O(3)···H(3*B*)—C(3)^{iii}	0.056 (5)	0.840 (4)	2.533	6.43
2		0.057 (6)	0.829 (4)	2.535	6.43
3		0.051 (7)	0.795 (5)	2.543	5.78
4		0.054 (7)	0.798 (4)	2.541	6.04
5		0.039 (5)	0.630 (3)	2.544	4.44
6		0.042 (11)	0.752 (4)	2.565	5.04
7		0.049 (3)	0.831 (2)	2.533	5.85
1	O(1)···H(2*A*)—C(2)^{vi}	0.052 (6)	0.766 (3)	2.490	5.78
2		0.053 (6)	0.780 (3)	2.494	5.91
3		0.037 (8)	0.714 (4)	2.505	4.59
4		0.044 (8)	0.734 (3)	2.504	4.99
5		0.038 (5)	0.662 (2)	2.565	4.22
6		0.031 (10)	0.586 (4)	2.477	3.62
7		0.051 (2)	0.789 (1)	2.490	5.77
1	O(6)···H(3*B*)—C(3)^{v}	0.046 (3)	0.645 (2)	2.685	4.86
2		0.046 (4)	0.645 (2)	2.686	4.86
3		0.041 (4)	0.618 (2)	2.707	4.33
4		0.043 (5)	0.630 (2)	2.704	4.46
5		0.042 (3)	0.548 (2)	2.750	4.06
6		0.042 (5)	0.601 (2)	2.718	4.36
7		0.040 (1)	0.650 (1)	2.685	4.45
1	O(2)···H(2*B*)—C(2)^{i}	0.041 (5)	0.501 (2)	2.657	3.81
2		0.041 (5)	0.497 (2)	2.660	3.81
3		0.047 (5)	0.477 (2)	2.680	4.07
4		0.049 (5)	0.463 (2)	2.678	4.07
5		0.035 (4)	0.426 (2)	2.767	3.13
6		0.042 (5)	0.415 (2)	2.760	3.49
7		0.041 (1)	0.459 (1)	2.657	3.61
1	O(5)···H(1*B*)—C(1)^{vii}	0.031 (4)	0.344 (1)	2.786	2.49
2		0.030 (4)	0.345 (2)	2.787	2.49
3		0.031 (4)	0.345 (2)	2.819	2.49
4		0.030 (5)	0.349 (2)	2.835	2.49
5		0.023 (3)	0.284 (2)	2.864	1.90
6		0.028 (6)	0.263 (2)	2.882	2.05
7		0.031 (1)	0.330 (1)	2.786	2.41

Symmetry operators: (i) $1/2 + x, y, 1/2 - z$; (ii) $x, 1/2 - y, -1/2 + z$; (iii) $1/2 + x, 1/2 - y, -z$; (iv) $1 - x, -1/2 + y, 1/2 - z$; (v) $1/2 - x, 1/2 + y, z$; (vi) $1 - x, 1/2 + y, 1/2 - z$; (vii) $1/2 - x, 1 - y, -1/2 + z$.

few hundredths e Å^{-3}, whereas, in the worst harmonic case, the difference was close to 1 e Å^{-3}. The biggest difference is observed for the N–O bonds, as expected. For these bonds, harmonic refinement at room temperature provided unreasonably high values of the electron density, Laplacian and the bond ellipticity. Topological bond orders for the covalent bonds (Howard & Lamarche, 2003; Tsirelson *et al.*, 2007) have been calculated from the electron-density values (ρ) and the principal electron-density curvatures (λ_1, λ_2, λ_3) at the bond critical points as $n_{topo} = a + b\lambda_3 + c(\lambda_1 + \lambda_2) + d\rho$. The following coefficients were used: for the N—O bond, $a = -0.628$, $b = 0.505$, $c = 0.448$, $d = 5.275$; for the N—N bond, $a = -0.755$, $b = 0.525$, $c = 2.041$, $d = 13.432$; for the N—C bond, $a = -0.851$, $b = 0.221$, $c = 0.715$, $d = 8.561$; for the C—H bonds, $a = 0.128$, $b = 0.246$, $c = 0.480$, $d = 4.926$. According to these bond-order values, the N—C and C—H bonds are single, as expected, with average bond-order values of 0.75 and 0.90, respectively.[10] The N—O bond order is 1.87 on average, and the N—N bond order is 1.27, both values reflecting the conjugation of the electron density in the —N—NO_2 fragment. There is a subtle difference between the pseudoequatorial and pseudoaxial N—N bonding, the equatorial bond being ∼0.04 Å shorter, and the bond order ∼0.13 higher. The bond-order agreement for both the 20 K refinements is very good. Using the 20 K values as a benchmark, significant improvement is obtained at other temperatures by inclusion of the anharmonic terms.

Bond critical points for the hydrogen bonds in the RDX crystal are listed in Table 4. In some of the refinements, critical points for different intramolecular O–H bonds [O(3)—H(2*A*) or O(1)—H(1*A*)] were found in the electron density, but no virial paths were confirmed (Bader, 1998). Thus, these interactions, not reproduced in all refinements, have been considered unreliable. Nine moderately strong intermolecular hydrogen bonds have been found in the RDX crystal with distances varying between 2.4 and 2.8 Å and dissociation energies from 8.53 to 2.49 kJ mol^{-1}.[10] Other bonding interactions, such as N—N, O—N and O—O, likely to be important for explosive materials, have been deposited. As in the case of the covalent bonds there is a quantitative difference between the properties at the critical points from different refinements

[10] After anharmonic refinements at 20 K.

Table 5
Atomic charges (q), volumes (Ω) and total electronic energies (H_e) integrated over atomic basins for RDX.

1: 20 K, anharmonic refinement; 2: 20 K, harmonic refinement; 3: 120 K, anharmonic refinement; 4: 120 K, harmonic refinement; 5: 298 K, anharmonic refinement; 6: 298 K, harmonic refinement; 7: theory; L_{err} = 0.0004 a.u. (1, 3, 5), 0.0005 a.u. (4, 7), 0.0006 a.u. (2), 0.004 a.u. (6), $L_{err} = (\Sigma L_\Omega{}^2/N_{atoms})^{1/2}$, L_Ω is the atomic integrated Lagrangian (Flensburg & Madsen, 2000). $\Omega_{unit\ cell}/8$ = 197.41 Å^3 (20 K), 199.66 Å^3 (120 K), 205.56 Å^3 (298 K). $H_e{}^{Crystal98}/8 = -897.248$ a.u.

Atom		q (e$^-$)	Ω (Å^3)	$-H_e$ (a.u.)	Atom		q (e$^-$)	Ω (Å^3)	$-H_e$ (a.u.)
O(1)	1	−0.419	15.34	74.840	N(6)	1	0.656	5.87	54.080
	2	−0.401	15.24	74.819		2	0.626	5.91	54.116
	3	−0.444	15.81	74.860		3	0.704	5.70	54.064
	4	−0.477	15.73	74.914		4	0.763	5.61	53.955
	5	−0.471	16.48	74.628		5	0.777	5.74	53.865
	6	−0.506	16.91	74.527		6	0.909	5.58	53.667
	7	−0.462	15.44	75.082		7	0.653	5.84	54.174
O(2)	1	−0.444	17.00	74.880	C(1)	1	0.450	7.75	37.988
	2	−0.430	16.88	74.866		2	0.409	7.91	38.040
	3	−0.478	17.52	74.886		3	0.559	7.31	37.896
	4	−0.471	17.26	74.893		4	0.490	7.62	37.945
	5	−0.531	18.33	74.824		5	0.420	8.18	37.980
	6	−0.529	18.05	75.283		6	0.477	8.43	37.904
	7	−0.434	17.02	75.061		7	0.491	7.35	37.994
O(3)	1	−0.429	16.83	74.863	C(2)	1	0.487	7.18	37.947
	2	−0.412	16.70	74.846		2	0.459	7.26	37.985
	3	−0.456	17.28	74.880		3	0.561	6.92	37.913
	4	−0.481	17.09	74.920		4	0.490	7.17	37.969
	5	−0.465	18.28	74.657		5	0.449	7.43	37.953
	6	−0.402	18.58	74.499		6	0.453	7.69	37.959
	7	−0.399	16.67	75.021		7	0.487	7.01	37.999
O(4)	1	−0.439	15.38	74.894	C(3)	1	0.503	7.04	37.919
	2	−0.419	15.32	74.871		2	0.474	7.16	37.957
	3	−0.476	15.74	74.918		3	0.462	7.43	37.949
	4	−0.494	15.72	74.974		4	0.421	7.59	37.975
	5	−0.484	16.36	74.695		5	0.442	7.41	37.937
	6	−0.570	16.63	74.876		6	0.508	7.31	37.880
	7	−0.433	15.40	75.104		7	0.472	6.98	38.024
O(5)	1	−0.420	15.74	74.834	H(1*A*)	1	0.199	4.93	0.484
	2	−0.395	15.68	74.805		2	0.220	4.94	0.460
	3	−0.472	16.28	74.863		3	0.081	5.09	0.611
	4	−0.457	16.16	74.872		4	0.203	4.85	0.488
	5	−0.439	16.89	74.535		5	0.159	5.28	0.504
	6	−0.628	17.08	75.966		6	0.232	4.33	0.465
	7	−0.439	16.01	75.086		7	0.133	5.01	0.566
O(6)	1	−0.438	14.51	74.880	H(1*B*)	1	0.113	6.07	0.540
	2	−0.435	14.47	74.895		2	0.123	6.05	0.532
	3	−0.457	14.86	74.849		3	0.118	6.20	0.527
	4	−0.504	14.92	74.941		4	0.040	6.52	0.590
	5	−0.523	15.52	74.781		5	0.147	6.31	0.490
	6	−0.515	16.21	74.820		6	−0.029	6.31	0.690
	7	−0.424	14.55	75.059		7	0.087	6.03	0.588
N(1)	1	−0.578	9.50	55.040	H(2*A*)	1	0.133	5.40	0.541
	2	−0.574	9.51	55.035		2	0.143	5.45	0.527
	3	−0.590	9.53	55.113		3	0.054	5.82	0.616
	4	−0.599	9.53	55.129		4	0.136	5.73	0.528
	5	−0.583	9.29	55.090		5	0.162	5.40	0.503
	6	−0.545	9.22	54.978		6	0.216	4.99	0.488
	7	−0.557	9.44	55.201		7	0.127	5.49	0.574
N(2)	1	−0.570	9.27	54.991	H(2*B*)	1	0.123	6.03	0.537
	2	−0.562	9.23	54.980		2	0.118	6.04	0.540
	3	−0.563	9.40	55.006		3	0.154	6.08	0.505
	4	−0.551	9.35	54.985		4	0.116	6.16	0.537
	5	−0.554	9.33	54.978		5	0.149	6.44	0.498
	6	−0.554	9.33	54.883		6	0.064	6.64	0.582
	7	−0.516	9.23	55.126		7	0.097	6.06	0.577
N(3)	1	−0.568	10.03	54.980	H(3*A*)	1	0.135	6.55	0.521
	2	−0.559	10.04	54.969		2	0.148	6.58	0.504
	3	−0.565	10.18	55.000		3	0.220	6.06	0.473
	4	−0.557	10.13	54.981		4	0.221	6.21	0.457
	5	−0.553	10.12	54.974		5	0.200	5.93	0.482
	6	−0.583	10.21	54.943		6	0.167	5.30	0.535
	7	−0.492	10.01	55.085		7	0.122	6.58	0.570

and at different temperatures, but no trend is observed. Quite logically, at room temperature the intermolecular hydrogen bonds are significantly longer, so the electron density, Laplacian and the dissociation energy have smaller values. By comparison with the discussion above, we assume that the values obtained from the anharmonic refinements are the most reliable.

Atomic properties integrated over atomic basins are listed in Table 5. The integrated Lagrangian for every atom was reasonably small, demonstrating the accuracy of the integrations after every refinement. The total sums of all atomic charges are very small, thus confirming that the molecules are practically electroneutral as required. The sums of the atomic volumes reproduce the unit-cell volume per molecule with an accuracy of 0.06–0.15%. As can be seen, the molecular electroneutrality and the 'average' integrated Lagrangian, L_{err}, are better for the anharmonic refinements at different temperatures. Note the negative charge of H(1*B*) and relatively low charge of H(2*B*) in the case of the harmonic refinement of the room-temperature data. Negative areas in the electron density could be the cause for these unreasonable values. Generally, there is a quantitative difference between atomic charges and volumes for the anharmonic and harmonic model refinements. The inclusion of anharmonic terms at 120 K and room temperature bring the integrated charges for O and N atoms into closer agreement with the 20 K anharmonic refinement. However, the situation is less clear for the C and H atoms.

The sums of the total electronic energies integrated over the atomic basins (Tsirelson & Stash, 2004; Zhurova *et al.*, 2004) agree reasonably well with the total energies calculated with wavefunctions using *CRYSTAL98* (within 0.06%). The RDX molecular electronic energy (H_e) per mole is 4.02–4.04 a.u. from different refinements, similar to that reported for HMX; this situates RDX in the middle of the range previously reported for other energetic compounds (Zhurova *et al.*, 2006, 2007).

The molecular dipole moment calculated from various refinements using monopole and dipole parameters of the multipole model (*A*) and integrated atomic charges and dipole moment components (*B*) is listed in Table 6. Our values are significantly larger than calculated theoretically in the crystal

Table 5 (continued)

Atom		q (e$^-$)	Ω (Å^3)	$-H_e$ (a.u.)	Atom		q (e$^-$)	Ω (Å^3)	$-H_e$ (a.u.)
N(4)	1	0.682	6.06	54.042	H(3*B*)	1	0.163	4.61	0.514
	2	0.655	6.11	54.080		2	0.169	4.64	0.502
	3	0.689	5.97	54.079		3	0.203	4.47	0.473
	4	0.747	5.89	53.964		4	0.211	4.50	0.482
	5	0.785	5.92	53.851		5	0.161	4.86	0.502
	6	0.750	6.07	53.891		6	0.138	4.79	0.531
	7	0.633	6.20	54.250		7	0.120	4.76	0.570
N(5)	1	0.653	6.02	54.102	Molecule	1	−0.008	197.12	893.419
	2	0.620	6.05	54.152		2	−0.022	197.17	893.483
	3	0.715	5.83	54.042		3	0.020	199.48	893.547
	4	0.773	5.80	53.928		4	0.019	199.55	893.426
	5	0.760	5.91	53.926		5	0.007	205.43	891.652
	6	0.848	5.66	53.713		6	−0.068	205.42	893.081
	7	0.653	6.05	54.178		7	−0.009	197.14	895.889

phase (7.4 D) by Tsiaousis *et al.* (2004) and the experimental value (5.8 D at 293 K in dioxane; McClellan, 1963).

Fig. 7 shows the electrostatic potential (ESP) mapped onto the molecular surface (ρ = 0.001 a.u.). Negative ESP areas are observed in the vicinity of the O atoms, and positive for H atoms, as expected. This ESP distribution is in good qualitative agreement with the earlier theoretically calculated electrostatic potential pattern for a single RDX molecule (Rice & Hare, 2002), and is typical for a moderately shock-sensitive explosive. The negative ESP distribution is less continuous than observed in HMX (Zhurova *et al.*, 2007), thus we do not observe a significant cooperative effect as was found in that case. All electrostatic potential distributions calculated from different refinements are qualitatively the same, except for the harmonic refinement at room temperature, which appears biased. In general, harmonic refinements result in a more extended range of ESP values.

5. Conclusion

We have demonstrated that, in order to obtain a meaningful and accurate electron-density distribution, anharmonicity of the atomic thermal motion has to be taken into account, especially in cases where the atomic displacements are relatively large, and at temperatures higher than provided by liquid helium. Neglecting anharmonicity may result in negative (and meaningless) regions of the total electron density, strongly distorted maps of the deformation electron density, the Laplacian and the electrostatic potential, unreasonable values for the properties at critical points and atomic integrated properties (especially charges) as well as higher R values, a more noisy residual density and poorer statistical distributions (scale factor and normal probability plots have been deposited). A similar conclusion has been recently obtained by Meindl *et al.* (2010) who studied the impact of anharmonic motion on the residual density and the Laplacian distribution. We suggest that the many reported studies with unusual deformations or polarizations of the electron density may well be due to unrecognized contributions from anharmonic displacements. Although the best solution to minimize this problem is the use of very low temperatures, improved results from ∼100 K data should be obtained by including anharmonic thermal motion in the refinement. The increase in the number of variables should be offset by including higher-order data than has historically been

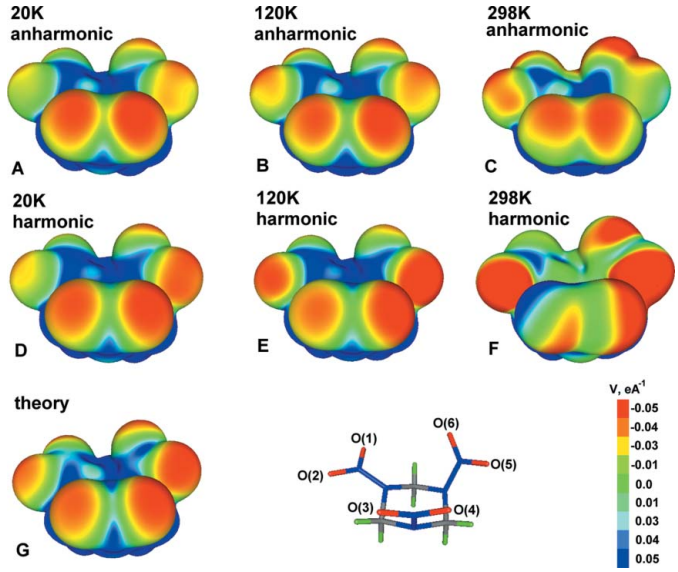

Figure 7
Electrostatic potential of a single RDX molecule taken from the solid state plotted on the molecular [$\rho(r)$ = 0.001 a.u.] surface: A: anharmonic model refinement at 20 K; B: anharmonic refinement at 120 K; C: anharmonic refinement at 298 K; D: harmonic model refinement at 20 K; E: harmonic refinement at 120 K; F: harmonic refinement at 298 K; G: multipole model refinement on theoretical data.

Table 6
RDX molecular dipole moment (Debye).

1: 20 K, anharmonic refinement; 2: 20 K, harmonic refinement; 3: 120 K, anharmonic refinement; 4: 120 K, harmonic refinement; 5: 298 K, anharmonic refinement; 6: 298 K, harmonic refinement; 7: theory; *A*: calculated from the multipole model parameters; *B*: calculated using charges and dipole moment components integrated over atomic basins.

	20 K				120 K				298 K				Theory	
	1*A*	1*B*	2*A*	2*B*	3*A*	3*B*	4*A*	4*B*	5*A*	5*B*	6*A*	6*B*	7*A*	7*B*
x	−6.23	−7.22	−5.92	−6.91	−7.90	−8.78	−6.48	−7.88	−8.65	−9.29	−2.63	−5.90	−7.10	−7.82
y	−1.08	−1.25	−1.12	−1.32	−1.39	−1.47	−0.76	−1.28	−1.72	−1.89	0.41	−1.94	−1.68	−1.78
z	4.71	5.12	4.81	5.21	4.32	4.64	5.55	5.88	3.62	3.89	9.21	9.84	4.50	4.91
Total	7.88	8.94	7.71	8.75	9.11	10.04	8.57	9.91	9.53	10.25	9.59	11.63	8.57	9.40

the case, this being easily accomplished with the current generation of instruments. In addition, we believe that H atoms can be (and, probably, should be) refined anisotropically, at least for relatively small molecules. The above conclusions are clearly contingent on the availability of suitably accurate experimental data.

In the α-RDX crystal the electron-density distribution for the $-NO_2$ groups is similar to other explosives with the oxygen lone-pair electron concentrations located close to perpendicular to the N—O bond vectors. Calculated topological bond orders reflect the conjugation of the electron density in the $-N-NO_2$ fragment, and also indicate the sensitivity to the conformation (axial *versus* equatorial) of the NO_2 group. Nine moderately strong intermolecular hydrogen bonds have been found and characterized in the RDX crystal along with nine other intermolecular bonding interactions, such as N—N, O—N and O—O. The RDX molecular electronic energy (H_e) per mole is 4.02–4.04 a.u., which is very close to the value reported for HMX.

Acknowledgment is made to the donors of the American Chemical Society Petroleum Research Fund for partial support of this research.

References

Allen, F. H. & Bruno, I. J. (2010). *Acta Cryst.* B**66**, 380–386.

Bader, R. F. W. (1990). *Atoms in Molecules: A Quantum Theory. The International Series of Monographs of Chemistry*, edited by J. Halpern & M. L. H. Green. Oxford: Clarendon Press.

Bader, R. F. W. (1998). *J. Phys. Chem. A*, **102**, 7314–7323.

Birkedal, H., Madsen, D., Mathiesen, R. H., Knudsen, K., Weber, H.-P., Pattison, P. & Schwarzenbach, D. (2004). *Acta Cryst.* A**60**, 371–381.

Blessing, R. H. (1987). *Crystallogr. Rev.* **1**, 3–58.

Blessing, R. H. (1995). *Acta Cryst.* B**51**, 816–823.

Chen, Y.-S. (2004). PhD Thesis, University of Toledo, Toledo, OH, USA.

Chen, Y.-S., Stash, A. I. & Pinkerton, A. A. (2007). *Acta Cryst.* B**63**, 309–318.

Choi, C. S. & Prince, E. (1972). *Acta Cryst.* B**28**, 2857–2862.

Ciezak, J. A., Jenkins, T. A., Liu, Z. & Hemley, R. J. (2007). *J. Phys. Chem. A*, **111**, 59–63.

Davidson, A. J., Oswald, I. D. H., Francis, D. J., Lennie, A. R., Marshall, W. G., Millar, D. I. A., Pulham, C. R., Warrenc, J. E. & Cumming, A. S. (2008). *CrystEngComm*, **10**, 162–165.

Espinosa, E. & Molins, E. (2000). *J. Chem. Phys.* **11**, 5686–5694.

Flensburg, C. & Madsen, D. (2000). *Acta Cryst.* A**56**, 24–28.

Hakey, P., Ouellette, W., Zubieta, J. & Korter, T. (2008). *Acta Cryst.* E**64**, o1428.

Hansen, N. K. & Coppens, P. (1978). *Acta Cryst.* A**34**, 909–921.

Hardie, M. J., Kirschbaum, K., Martin, A. & Pinkerton, A. A. (1998). *J. Appl. Cryst.* **31**, 815–817.

Harris, P. M. & Reed, P. T. (1959). AFOSR-TR-59–165, Ohio State University Research Foundation, Columbus, Ohio.

Hirshfeld, F. L. (1976). *Acta Cryst.* A**32**, 239–244.

Howard, S. T. & Lamarche, O. (2003). *J. Phys. Org. Chem.* **16**, 133–141.

Ivanov, Y., Zhurova, E. A., Zhurov, V. V., Tanaka, K. & Tsirelson, V. (1999). *Acta Cryst.* B**55**, 923–930.

Iversen, B. B., Larsen, F. K., Pinkerton, A. A., Martin, A., Darovsky, A. & Reynolds, P. A. (1999). *Acta Cryst.* B**55**, 363–374.

Kirschbaum, K., Martin, A., Parrish, D. & Pinkerton, A. A. (1999). *J. Phys. Condens. Matter*, **11**, 4483–4490.

Kubicki, M., Borowiak, T., Ditkiewicz, G., Souhassou, M., Jelsch, C. & Lecomte, C. (2002). *J. Phys. Chem.* **106**, 3706–3714.

McClellan, A. L. (1963). *Tables of Experimental Dipole Moments.* San Francisco: W. H. Freeman.

Madsen, A. Ø. (2006). *J. Appl. Cryst.* **39**, 757–758.

Madsen, A. Ø, Sørensen, H. O., Flensburg, C., Stewart, R. F. & Larsen, S. (2004). *Acta Cryst.* A**60**, 550–561.

Mallinson, P. R., Koritsanszky, T., Elkaim, E., Li, N. & Coppens, P. (1988). *Acta Cryst.* A**44**, 336–343.

Meindl, K., Herbst-Irmer, R. & Henn, J. (2010). *Acta Cryst.* A**66**, 362–371.

Messerschmidt, M., Wagner, A., Wong, M. W. & Luger, P. (2002). *J. Am. Chem. Soc.* **124**, 732–733.

Munshi, P., Madsen, A. Ø., Spackman, M. A., Larsen, S. & Destro, R. (2008). *Acta Cryst.* A**64**, 465–475.

Otwinowski, Z. & Minor, W. (1997). *Methods Enzymol. A*, **276**, 307–326.

Piccoli, P. M. B., Koetzle, T. F., Schultz, A. J., Zhurova, E. A., Stare, J., Pinkerton, A. A., Eckert, J. & Hadzi, D. (2008). *J. Phys. Chem. A*, **112**, 6667–6677.

Restori, R & Schwarzenbach, D. (1996). *Acta Cryst.* A**52**, 369–378.

Ribaud, L., Wu, G., Zhang, Y. & Coppens, P. (2001). *J. Appl. Cryst.* **34**, 76–79.

Rice, B. M. & Hare, J. J. (2002). *J. Phys. Chem. A*, **106**, 1770–1783.

Ritchie, J. P., Zhurova, E. A., Martin, A. & Pinkerton, A. A. (2003). *J. Phys. Chem. B*, **107**, 14576–14589.

Roversi, P. & Destro, R. (2004). *Chem. Phys. Lett.* **386**, 472–478.

Saunders, V. R., Dovesi, R., Roetti, C., Causà, M., Harrison, N. M., Orlando, R. & Sicovich-Wilson, C. M. (1998). *CRYSTAL98 User's Manual.* University of Torino, Torino, Italy.

Scheins, S., Zheng, S.-L., Benedict, J. B. & Coppens, P. (2010). *Acta Cryst.* B**66**, 366–372.

Sheldrick, G. M. (2008). *Acta Cryst.* A**64**, 112–122.

Simpson, R. L., Urtiew, P. A., Omellas, D. L., Moody, G. L., Scribner, K. J. & Hoffman, D. M. (1997). *Propellants Explos. Pyrotech.* **22**, 249–255.

Stash, A. & Tsirelson, V. (2002). *J. Appl. Cryst.* **35**, 371–373.

Stash, A. I. & Tsirelson, V. G. (2005). *Crystallogr. Rep.* **50**, 202–209.

Storm, C. B., Stine, J. R. & Kramer, J. F. (1990). *Chemistry and Physics of Energetic Materials*, edited by S. N. Bulusu, pp. 605–639. Dordrecht: Kluwer Academic Publishers.

Svensson, M., Humbel, S., Froese, R. D. J., Matsubara, T., Sieber, S. & Morokuma, K. (1996). *J. Phys. Chem.* **100**, 19357–19363.

Tsiaousis, D., Munn, R. W., Smith, P. J. & Popelier, P. L. A. (2004). *Chem. Phys.* **305**, 317–323.

Tsirelson, V. & Stash, A. (2004). *Acta Cryst.* A**60**, 418–426.

Tsirelson, V., Stash, A., Kohout, M., Rosner, H., Mori, H., Sato, S., Lee, S., Yamamoto, A., Tajima, S. & Grin, Y. (2003). *Acta Cryst.* B**59**, 575–583.

Tsirelson, V. G., Bartashevich, E. V., Stash, A. I. & Potemkin, V. A. (2007). *Acta Cryst.* B**63**, 142–150.

Vladimiroff, T. & Rice, B. M. (2002). *J. Phys. Chem. A*, **106**, 10437–10443.

Volkov, A., Abramov, Y., Coppens, P. & Gatti, C. (2000). *Acta Cryst.* A**56**, 332–339.

Volkov, A., Macchi, P., Farrugia, L. J., Gatti, C., Mallinson, P., Richter, T. & Koritsanszky, T. (2006). *XD2006 – A Computer Program Package for Multipole Refinement, Topological Analysis of Charge Densities and Evaluation of Intermolecular Energies from Experimental or Theoretical Structure Factors.* University at Buffalo, State University of New York, NY, USA; University of Milano, Italy; University of Glasgow, UK; CNRISTM, Milano, Italy; Middle Tennessee State University, TN, USA.

Whitten, A. E. & Spackman, M. A. (2006). *Acta Cryst.* B**62**, 875–888.

Zhurov, V. V., Zhurova, E. A., Chen, Y.-S. & Pinkerton, A. A. (2005). *J. Appl. Cryst.* **38**, 827–829.

Zhurov, V. V., Zhurova, E. A. & Pinkerton, A. A. (2011). In preparation.

Zhurova, E. A., Ivanov, Y., Zavodnik, V. & Tsirelson, V. (2000). *Acta Cryst.* B**56**, 594–600.
Zhurova, E. A., Martin, A. & Pinkerton, A. A. (2002). *J. Am. Chem. Soc.* **124**, 8741–8750.
Zhurova, E. A. & Pinkerton, A. A. (2001). *Acta Cryst.* B**57**, 359–365.
Zhurova, E. A., Stash, A. I., Tsirelson, V. G., Zhurov, V. V., Bartashevich, E. V., Potemkin, V. A. & Pinkerton, A. A. (2006). *J. Am. Chem. Soc.* **128**, 14728–14734.
Zhurova, E. A. & Tsirelson, V. G. (2002). *Acta Cryst.* B**58**, 567–575.
Zhurova, E. A., Tsirelson, V. G., Stash, A. I., Yakovlev, M. V. & Pinkerton, A. A. (2004). *J. Phys. Chem. B*, **108**, 20173–20179.
Zhurova, E. A., Zhurov, V. V. & Pinkerton, A. A. (2007). *J. Am. Chem. Soc.* **129**, 13887–13993.
Zhurova, E. A., Zhurov, V. V. & Tanaka, K. (1999). *Acta Cryst.* B**55**, 917–922.